Vacuum Membrane Distillation: Experiments and Modeling

Serena Bandini, Aldo Saavedra, and Giulio Cesare Sarti
Dipartimento di Ingegneria Chimica, Mineraria e delle Tecnologie Ambientali, Universitá degli Studi di Bologna, I-40136 Bologna, Italy

Vacuum membrane distillation is a membrane-based separation process considered here to remove volatile organic compounds from aqueous streams. Microporous hydrophobic membranes are used to separate the aqueous stream from a gas phase kept under vacuum. The evaporation of the liquid stream takes place on one side of the membrane, and mass transfer occurs through the vapor phase inside the membrane. The role of operative conditions on the process performance is widely investigated in the case of dilute binary aqueous mixtures containing acetone, ethanol, isopropanol, ethylacetate, methylacetate, or methylterbutyl ether. Temperature, composition, flow rate of the liquid feed, and pressure downstream the membrane are the main operative variables. Among these, the vacuum-side pressure is the major design factor since it greatly affects the separation efficiency. A mathematical model description of the process is developed, and the results are compared with the experiments. The model is finally used to predict the best operative conditions in which the process can work for the case of benzene removal from waste waters.

Introduction

Vacuum membrane distillation (VMD) is a new membrane-based separation process which has been proposed for several purposes such as the production of ultrapure water from salt solutions, the extraction of dissolved gases, and the selective removal of volatile solutes from aqueous streams (Bandini et al., 1988, 1992; Sarti et al., 1993). In particular, VMD was also investigated as a tool for the continuous removal of ethanol from fermentation broths in order to increase the bioreactor productivity (Hofman et al., 1987; Aptel et al., 1988).

The process is based on the use of microporous hydrophobic membranes, mostly made of PTFE and polypropylene, which are not wetted by aqueous mixtures. One side of the membrane is in direct contact with an aqueous liquid feed, while a gaseous phase downstream the membrane (the distillate or the permeate side) is kept at a pressure below the equilibrium vapor pressure of the feed itself (Figure 1c). Due to the liquid repulsing properties of the membrane material, as long as a pressure is maintained lower than the minimum entry value, a liquid-vapor interface exists at the pore entries.

Like all the membrane distillation processes (Andersson et al., 1985; Jonsson et al., 1985; Sarti et al., 1985; Gostoli et al., 1987; Schofield et al., 1987), VMD is essentially a thermal

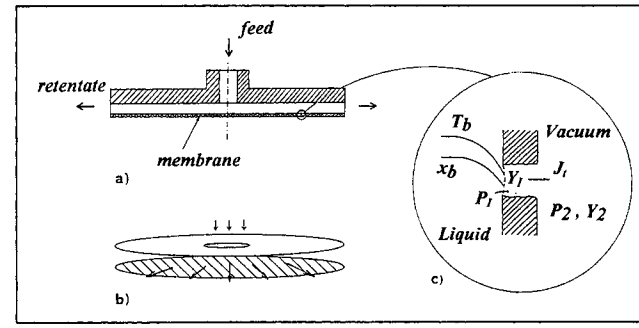

Figure 1. VMD process.

(a) Liquid side semicell; (b) flow pattern in the liquid side; (c) detail of the porous membrane showing the temperature and concentration profiles, with reference to the organic compounds.

Correspondence concerning this article should be addressed to G. C. Sarti.
Current address of A. Saavedra: Departamento de Ingeniería Quimíca, Universidad de Santiago de Chile, Av Lib. Bdo. O'Higgins 3363, Santiago, Chile.

process: evaporation of the liquid mixtures takes place at the L-V interface and the vapors diffuse through the membrane pores.

The vapor stream permeated from the membrane apparatus is then condensed under vacuum. In the case of aqueous mixtures containing volatile organic compounds (VOCs) partially miscible with water, two liquid phases are obtained in the condenser: the supernatant organic is recovered and the water stream containing organic traces is recirculated to the membrane separator. In the case in which the organic compound is completely miscible with water, a concentrated liquid stream is obtained from the condenser.

The VMD process can be thus applied both in order to simply remove an organic component from wastewater streams and to recover valuable products to a high degree of purity.

Since the nonwettability of the porous membrane is the basic requirement for the process, the same hydrophobic membrane can be used for the VMD extraction of a broad variety of volatile organic components from aqueous mixtures; the process separation is not associated to the selective solubility of the organic components in the membrane material.

Generally, only aqueous solutions, usually containing VOC at a concentration below 10 wt. %, can be separated through this process. Indeed, only for dilute solutions the penetration pressure is sufficiently high to make the process feasible on an industrial scale (Sarti et al., 1989). Moreover, the treatment of solutions, containing VOC with limited solubility in water, can be safely used only by preventing the formation of an organic liquid phase which otherwise would wet the membrane.

The process can be taken under consideration in alternative to conventional separations such as carbon adsorption, distillation, and steam distillation.

In comparison with the conventional techniques, one of the major advantages is the possibility of working at relatively low evaporation temperatures, typically below 50–60°C. In that case, also low value energy sources can be clearly used to supply the heat required for the evaporation. The membrane modules commercially available, both in the hollow fiber and spiral wound configurations, are endowed with surface areas per unit volume at least three or four times larger than in conventional gas/liquid contacting equipments (Yang and Cussler, 1986). Further advantages of VMD operations are represented by the possibility of maintaining under vacuum only a very limited volume of the membrane equipment and not the entire apparatus. Finally, the use of membrane modules makes the plant scale-up straightforward, in view of the modularity of the system.

With reference to the separation costs, VMD is also found to be economically comparable (Sarti et al., 1993) with other membrane alternatives, such as pervaporation (Wijmans et al., 1990; Lipski and Cotè, 1990).

The working pressures in the gaseous phase are well below the atmospheric values, and the molecular mean free path of the permeants is substantially larger than the pore sizes of the membranes typically used. As a consequence, mass transfer through the membrane is generally dominated by the Knudsen mechanism (Dullien, 1979). The process selectivity is therefore associated both to the liquid vapor equilibrium and to the relative Knudsen diffusivity of the permeants. As the molecular weight of the organic permeants is sufficiently larger with respect to water, the Knudsen separation is always unfavorable to the process; the upper limit for the permeate composition is thus represented by the L-V equilibrium value corresponding to the feed composition.

Since an evaporation takes place at the membrane pore entries, also heat- and mass-transfer resistances through the liquid phase affect the process selectivity.

The technical feasibility of the process was established and a detailed model containing no adjustable parameters was developed and successfully compared with the experimental data with reference to the hollow fibers configuration (Sarti et al., 1993).

In this work a rather extensive study is presented for the removal of different VOCs from aqueous streams. In particular, dilute binary aqueous mixtures are considered which contain acetone, ethanol, isopropanol, ethylacetate, methylacetate, and methylterbutyl ether. Experimental measures of the membrane permeability are also reported.

The downstream pressure and the feed flow rate were identified as the major design quantities; a detailed experimental study has been completed in order to clarify the influence of those parameters on the process performance.

The VMD model is tested for flat membranes located in circular cells with radial flow, and used to predict the best operative conditions in which the process can work, for the reference case of benzene removal from waste waters.

Experimental Methods

Feed solutions

Dilute binary solutions in water of acetone, ethanol, isopropanol (IPA), ethylacetate (EtAc), methylacetate (MeAc), and methylterbutyl ether (MTBE) were prepared from reagent-grade organics and distilled water.

Membrane apparatus

Experimental tests were performed using flat PTFE membranes from Gelman Instruments Co. as TF200; the membrane properties are reported in Table 1.

The membrane is located in the middle of a circular cell of 74 mm diameter and divides it in two chambers 2 mm deep (Figure 1a). A 25 μm paper filter and a polypropylene mesh support the membrane and prevent strain and breakage against the cell wall. The feed enters the center of the liquid side semicell perpendicularly to the membrane and flows outwards in the radial direction (Figure 1b). In such a configuration the membrane area useful for the process is 43 cm^2.

Experimental setup

The apparatus used in the experimental tests was quite similar to a PV setup. The liquid was continuously fed to the membrane cell from a reservoir, sufficiently large to keep the concentration nearly constant. Cold traps refrigerated by liquid nitrogen were used to condense and recover the permeating vapors. The permeate composition was measured by a refractometer for the case of binary solutions of ethanol, ace-

Table 1. Membrane Properties

	Pore Size (μm)	Porosity	Thickness (μm)	ID (mm)	K_m (25°C) $mol^{1/2}\cdot s\cdot m^{-1}\cdot kg^{-1/2}$
TF200(†) PTFE	0.2	60%	60	flat	$3.15*10^{-5}$*
Accurel Q3/2(‡) PP	0.2	75%	200	0.6	$4.0*10^{-6}$**

*measured.
**predicted by Eq. 2 ($\chi = 2$).
†from Gelman.
‡from AKZO.

tone, and isopropanol, and by a gas chromatograph with a thermal conductivity detector for the case of binary solutions of ethylacetate, methylacetate, and methylterbutyl ether.

Experimental conditions

Experiments were performed in order to investigate the role of the main process variables. For each binary mixture, the influence of temperature, composition, and recirculation rate in the liquid side and of pressure in the vacuum side were studied. Temperature, composition, and recirculation rate were varied in the range 25 to 35°C, 2 to 10 wt. %, 0.05 to 3 L/min, respectively. The downstream pressure range examined strictly depends on the mixture under investigation: the value of the downstream pressure must be kept below the equilibrium vapor pressure of the feed, and thus very different pressure ranges can be used for the VMD process. In Table 2, the pressure values at which the experiments were performed are reported for each binary mixture investigated.

In all runs only minor differences between inlet and outlet temperatures and compositions in the liquid phase were observed; indeed, the evaporation flux was always smaller than 1% with respect to the liquid flow rate. Therefore, in the elaboration of the experimental data temperature and composition in the liquid bulk were taken as constants and equal to the respective inlet values.

Experimental Results and Discussion

Among the process variables investigated in the experimental tests, three quantities provided very important results for the process performance: the membrane permeability, the pressure downstream the membrane, and the flow rate in the liquid phase. The experimental results are reported here, in which the influence of each quantity will be considered in detail.

Membrane permeability

Membrane permeability to the species i $K_m\sqrt{M_i}$ was defined according to Eq. 1

Table 2. VMD of Aqueous Solutions: Vacuum-Side Pressure

VOC in Water	Pressure mbar
acetone	10 ÷ 80
ethanol	10 ÷ 30
IPA	10 ÷ 70
EtAc	20 ÷ 95
MeAc	25 ÷ 150
MTBE	20 ÷ 140

$$N_i = K_m\sqrt{M_i}\,\Delta P_i \tag{1}$$

where N_i is the mass flux ($kg\cdot m^{-2}\cdot s^{-1}$), ΔP_i the partial pressure difference across the membrane (Pa), and M_i the molar mass of the permeating species ($kg\cdot mol^{-1}$), respectively. Subscript i is the ith component (VOC).

Making use of the gas kinetic theory applied to a fluid diffusing inside the pore of a solid medium (Dullien, 1979), the permeability coefficient K_m ($s\cdot mol^{1/2}\cdot m^{-1}\cdot kg^{-1/2}$) can be obtained as follows

$$K_m = \frac{4\epsilon d_p}{3\chi\delta(2\pi RT)^{1/2}} \tag{2}$$

Apparently, the permeability coefficient K_m depends upon temperature and on the membrane properties only, in terms of pore-size distribution d_p (m), thickness δ (m), void fraction ϵ, and tortuosity factor χ. It can thus be calculated independently of the permeating species, however, owing to the nonuniform pore-size distribution of the membrane, it is more convenient and reliable to measure K_m directly. Air permeation experiments at different downstream pressures and at different average pressures are the most simple way to obtain the K_m values for different membranes. R is the universal gas constant ($J\cdot mol^{-1}\cdot K^{-1}$).

In Figure 2a air flux is reported vs. pressure difference across the TF200 membrane, with reference to experiments with different membrane samples at 20°C; the downstream pressure was varied in the range 3.5 to 315 mbar. The linear behavior observed indicates that viscous flow in the pores is negligible with respect to Knudsen diffusion. According to Eq. 1, the slope of the straight line is therefore related to K_m, the value measured for the TF200 membrane is $K_m = 3.15\times10^{-5}$ $mol^{1/2}\cdot s\cdot m^{-1}\cdot kg^{-1/2}$.

In Figure 2b the permeability coefficients calculated according to Eq. 1 for each experimental run are reported vs. the Knudsen number (Kn) evaluated at the average pressure values existing across the membrane; Kn is defined as the ratio between the air mean molecular free path and the nominal membrane pore diameter. Apparently, at the higher Kn numbers, that is, at lower pressures, the membrane permeability K_m is nearly constant; on the contrary, at the lower Kn number, occurring at the higher pressures, K_m increases as the downstream pressure increases. In the pressure ranges investigated in the VMD experiments (Table 1) the Kn number belongs to the range 5 to 50; the constant value for the permeability coefficient $K_m = 3.15\times10^{-5}$ $mol^{1/2}\cdot s\cdot m^{-1}\cdot kg^{-1/2}$ can be therefore considered correctly in all VMD tests.

The K_m coefficient slightly depends on temperature: according to Eq. 2 over the temperature range investigated from

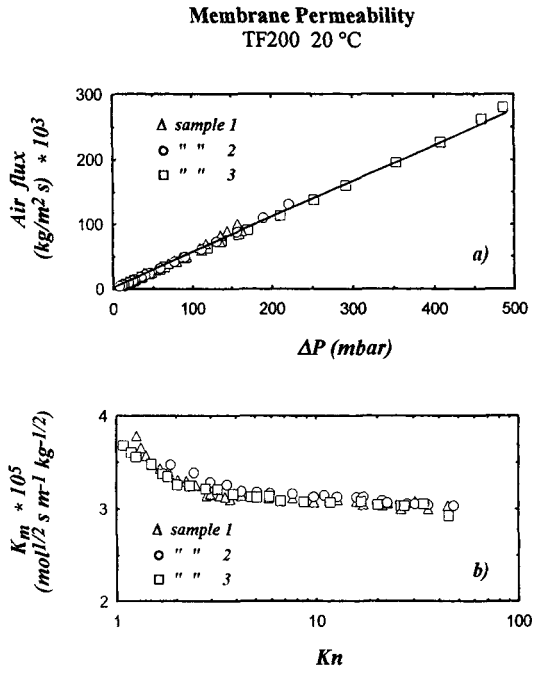

Figure 2. Permeability tests of TF200 membrane.

(a) Air flux vs. the driving force; (b) permeability coefficient vs. the Knudsen number.

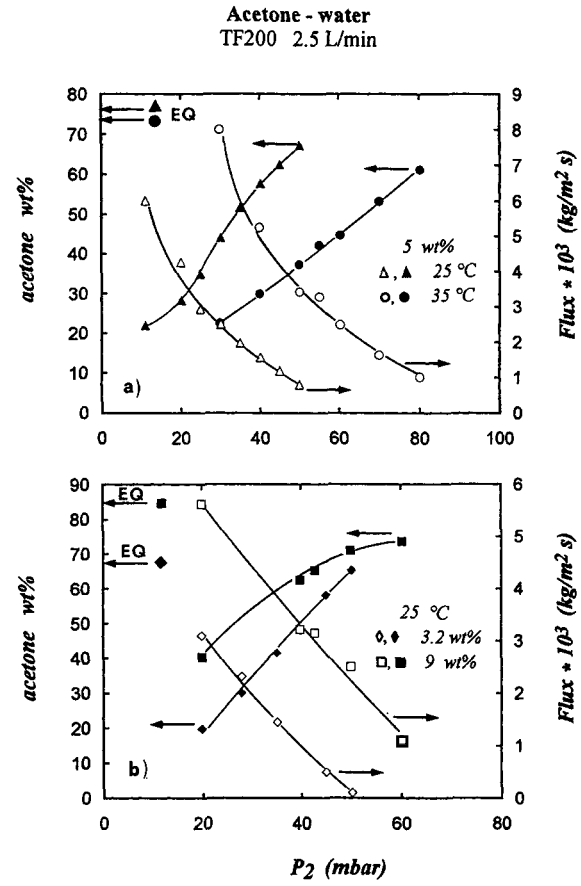

Figure 3. VMD of acetone-water mixtures at various feed temperatures and compositions: distillate composition and total flux vs. downstream pressure.

EQ represents the vapor composition in equilibrium with the liquid feed.

20°C to 35°C, only a 2% change in K_m occurs due to temperature changes. The value measured in air at 20°C can be therefore used with confidence in the elaboration of all the data obtained.

It should be pointed out that the measured value of K_m is remarkably close to the kinetic theory value of 2.15×10^{-5} $mol^{1/2} \cdot s \cdot m^{-1} \cdot kg^{-1/2}$ calculated at 20°C assuming a unity tortuosity factor. However, the uncertainty about the tortuosity makes the above experimental measures necessary.

Pressure in vacuum side

Figures 3 to 5 show the experimental results obtained in VMD of binary solutions of VOC in water: total transmembrane fluxes and distillate compositions are reported vs. the downstream pressure at various feed temperatures and compositions; for comparison, in the same figures an arrow indicates the liquid-vapor equilibrium conditions with respect to the liquid feed.

For all the mixtures tested, the following qualitative features were observed:

(1) As the downstream pressure increases, the transmembrane flux decreases and, correspondingly, the VOC composition in the distillate increases;

(2) The distillate VOC compositions are lower than the corresponding equilibrium values with the feed which are approached at the higher pressures;

(3) For given downstream pressure conditions, at higher temperatures higher fluxes and lower distillate VOC compositions are obtained;

(4) For given downstream pressure conditions and at the same feed temperature at higher VOC concentrations in the liquid feed, higher fluxes and higher distillate compositions are measured.

The behavior observed at points 1 and 2 shows the presence of two concomitant effects in determining the process performance: Knudsen separation in the membrane and polarization phenomena in the liquid phase.

As the molar mass of the organic permeants is larger with respect to that of water, the Knudsen separation is certainly always unfavorable to the process; as a consequence, the upper limit for the permeate composition is represented by the L-V equilibrium value corresponding to the feed conditions, as shown from the experiments.

Moreover, the lower VOC distillate compositions, that is, the lower separation factors, are observed especially at the lower-pressure values which correspond to the higher fluxes; that is characteristic of a significant effect of temperature and concentration polarization within the liquid phase. Indeed, since evaporation takes place at the L-V interface located on the membrane, temperature and VOC concentration at the interface are generally different and lower than the corresponding liquid bulk values.

The relative importance of the Knudsen separation and of the polarization effects on the process performance is thus different from case to case: it depends upon the permeating species, on the working pressure, and on the fluodynamic

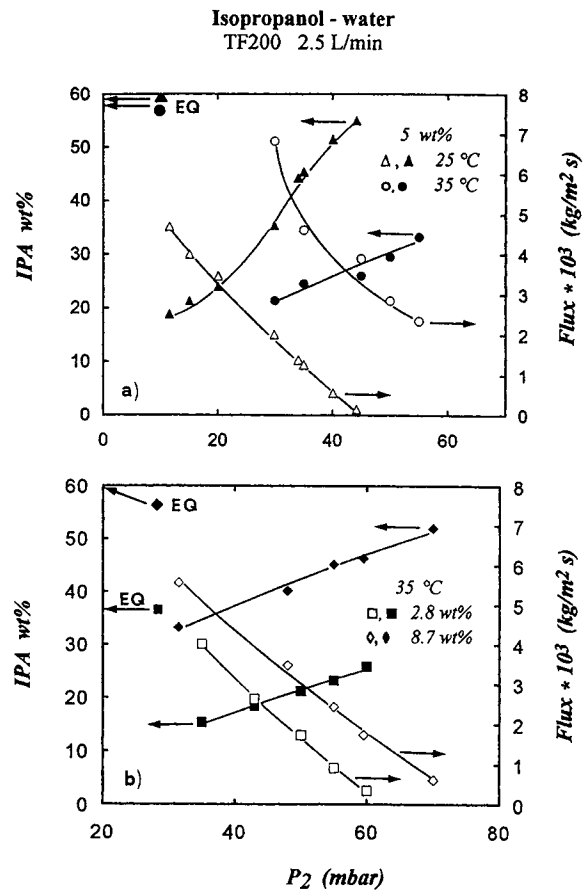

Figure 4. VMD of IPA-water mixtures at various feed temperatures and compositions: distillate composition and total flux vs. downstream pressure.

EQ represents the vapor composition in equilibrium with the liquid feed.

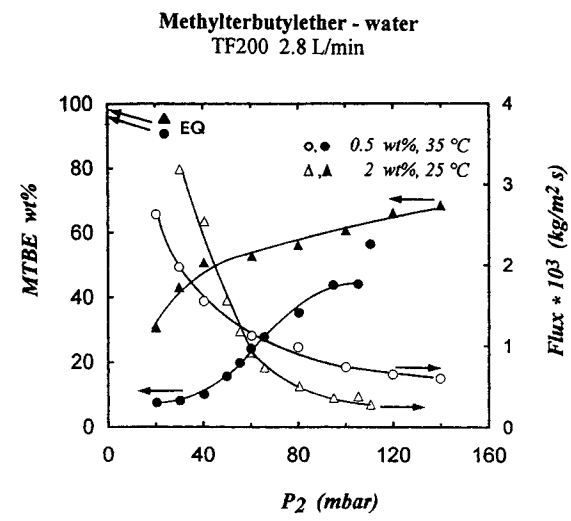

Figure 5. VMD of MTBE-water mixtures at various feed temperatures and compositions: distillate composition and total flux vs. downstream pressure.

EQ represents the vapor composition in equilibrium with the liquid feed.

conditions, that is, on the flow rate in the liquid feed. The influence of the feed flow rate will be discussed in detail in the next section.

It is important to notice the appreciable effect of the downstream pressure on the VOC distillate concentration; higher-pressure values may lead to rather high organic content in the vapor phase such as up to 68 wt. % for MTBE and 67 wt. % for acetone from liquid feeds containing 2 wt. % MTBE and 5 wt. % acetone, respectively. That results from a significant reduction of the driving force for water flux as the pressure increases, whereas the driving forces for the VOCs undergo only a smaller decrease.

The effect is clearly put in evidence in Figures 6 and 7 in which the overall flux as well as the fluxes of water and organic component are reported vs. the downstream pressure, for the cases of VMD of aqueous mixtures containing MeAc and EtAc, respectively. At low-pressure values the water flux is very large with respect to the solute flux and approaches the total flux, so that the distillate has a low solute concentration and a very high water content; at high-pressure values, on the contrary, the water flux rapidly decreases so that the organic concentration becomes dominant. The behavior is observed for all the organic compounds highly volatile with respect to water, presenting equilibrium compositions in the vapor phase above 50 wt. %, at least.

The effect of temperature on VMD performance appears very interesting: at higher temperatures there is a broader pressure range at which VMD can be effective, due to the higher vapor pressures of the feed. As is typical for all membrane distillation processes, at higher temperatures higher fluxes are obtained with respect to the lower-temperature cases for any single value of the distillate compositions. As a numerical example, it can be noted that in the case of VMD

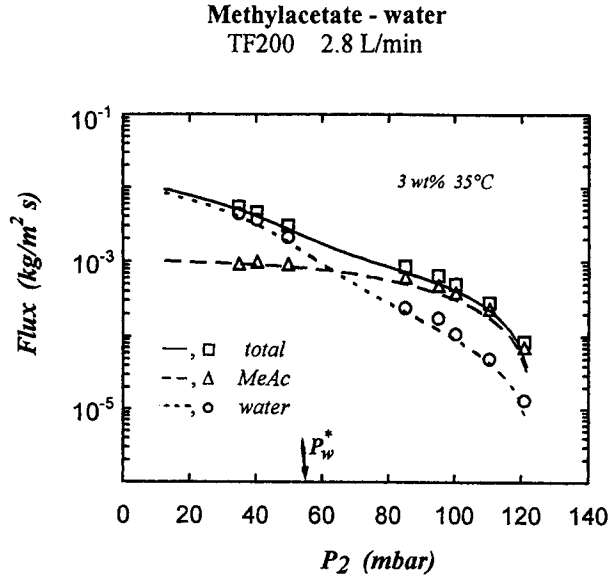

Figure 6. Model predictions (lines) vs. experimental data (symbols) in VMD of MeAc-water mixtures: total, water, and organic fluxes vs. downstream pressure.

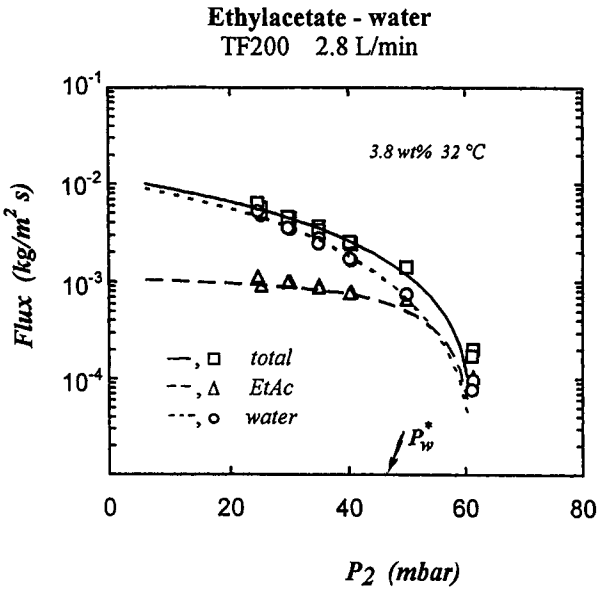

Figure 7. Model predictions (lines) vs. experimental data (symbols) in VMD of EtAc-water mixtures: total, water, and organic fluxes vs. downstream pressure.

of 5 wt. % acetone-water mixtures (Figure 3a) an experimental distillate composition of nearly 30 wt. % was obtained working both at 25°C and 20 mbar and 35°C and 40 mbar; the transmembrane fluxes were measured as 4.3×10^{-3} and 5.2×10^{-3} kg·m^{-2}·s^{-1}, respectively.

The effect of the organic composition in the feed follows the obvious expectations: for a given temperature at higher compositions in the liquid feed, higher VOC compositions in the distillate are obtained; correspondingly, higher equilibrium vapor pressures exist at the L-V interface, which give rise to higher permeate fluxes.

Feed flow rate

The experimental results thus far presented are qualitatively suggestive of the important role of the polarization phenomena in the liquid phase on the process performance. Such effects depend mainly upon the fluodynamic conditions in the liquid phase and can be experimentally investigated by changing the feed flow rate.

Experiments were performed testing solutions containing different organic compounds; in Figure 8 the results obtained in VMD of dilute mixtures containing IPA are reported as an example. (In Figure 8 ω is the mass fraction.) The transmembrane fluxes of the organic component and of water are separately reported vs. the feed flow rate in the liquid phase, at various feed temperatures, compositions and downstream pressures.

For all the mixtures tested, the same qualitative behavior is observed:

(1) Both the organic and water flux significantly increase with the feed flow rate, especially so in the low flow rate range;

(2) The influence of the feed flow rate on the organic flux is much higher than on the water flux.

As numerical examples, in the case of VMD of 5 wt. % IPA-water mixtures at 20 mbar and 25°C (Figure 8) the organic and water fluxes increase nearly 320% and 30%, respectively, as the recirculation rate increases from 0.05 to 2.6 L/min; in the case of VMD of 3 wt. % EtAc-water mixtures at 25 mbar and 30°C, EtAc and water fluxes increase nearly 340% and 50%, respectively, as the recirculation rate increases from 0.09 to 2.9 L/min.

The behavior observed clearly shows the significant importance of the transport phenomena in the liquid phase in determining the process performance; as the feed flow rate increases, the heat- and mass-transfer resistances in the liquid phase decrease and the flux of each component increases.

At the present stage of the work, from those data it is not possible to predict which resistance controls the flux of each

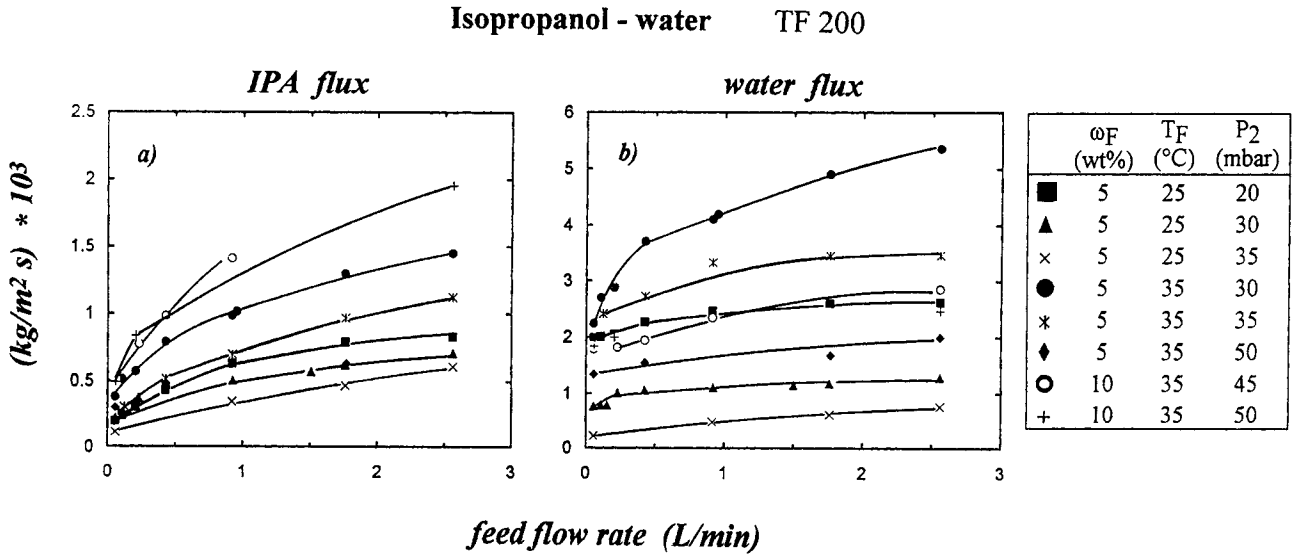

Figure 8. VMD of IPA-water mixtures at various feed conditions and downstream pressures: IPA and water fluxes vs. feed flow rate.

component (whether the heat or mass transfer in the liquid or the mass transfer through the membrane) nor if there is a single resistance controlling the whole process. To that purpose, a detailed analysis of the transport resistances involved in the process is necessary and it will be presented in a subsequent article. Anyway, some qualitative remarks can also be made on the basis of the experimental observations. The strong influence of the feed flow rate on the organic flux shows that certainly the mass-transfer resistance through the membrane is not the limiting factor, since otherwise no effect of the recirculation rate would be observed. For water flux, on the contrary, the relatively weak influence of the recirculation rate indicates that the membrane resistance may not be negligible.

In addition, since the feed mixtures inspected are rather dilute in the VOC, the mole fraction of water within the liquid phase does not change appreciably and is always larger than 0.98; thus, mass-transfer resistance in the liquid phase likely does not contribute to the water flux. Therefore, the observed dependence of the water flux from the feed flow rate is to be attributed to the heat-transfer resistance within the liquid. It is vice versa for the flux of the organic component. The heat- and mass-transfer resistances in the liquid phase are both important, and this justifies the high sensitivity on feed flow rate variations.

Model and Predictions

Theory

The model describing VMD has been widely investigated and its ability to represent the separation process has been already well documented (Sarti et al., 1993). For the sake of clarity, the equations describing the main physical phenomena involved in the process are reported hereafter.

Mass transfer in membrane distillation processes generally occurs by diffusive and convective transport of vapors through the microporous membrane. Since for all the typical operative conditions the membrane pore size is well below the mean free molecular path of the permeating species, in the VMD process Knudsen diffusion is dominant with respect to molecular diffusion. On the other hand, as a total pressure gradient is maintained across the membrane, the nonseparative Poiseuille flow should also be taken into account. However, as has been observed from Figure 2a, in this process the viscous contribution to the total flux is quite negligible with respect to the diffusion. Therefore, Knudsen diffusion is the prevailing mechanism of mass transport through the membrane. As a consequence, the molar flux of a permeating specie J_i (mol·m^{-2} s^{-1}) is linearly related to its partial pressure difference across the membrane

$$J_i = \frac{K_m}{\sqrt{M_i}}(P_1 Y_{i,1} - P_2 Y_{i,2}) \tag{3}$$

where K_m is the permeability coefficient defined in Eq. 1. Y is the mole fraction in the vapor phase.

By taking the sum over all the components, the total molar flux J_t (mol·m^{-2} s^{-1}) can be easily expressed as

$$J_t = \frac{K_m}{\sqrt{M}}(P_1 - P_2) \tag{4}$$

where M (kg·mol^{-1}) is a suitable average molecular weight in the permeating stream, defined as

$$\sqrt{M} = \sum_i \frac{J_i}{J_t}\sqrt{M_i} \tag{5}$$

The heat required for the interfacial evaporation is supplied by the heat flux through the liquid stream; a simple balance across the evaporation surface gives

$$\sum_i J_i \lambda_i = h(T_b - T_I) \tag{6}$$

where h is the heat-transfer coefficient in the liquid phase (W·m^{-2}·K^{-1}). In writing Eq. 6 the convective heat transfer within the gaseous phase was not included since its contribution, though nonzero, is indeed negligible. λ is the molar latent heat of vaporization (J·mol^{-1}).

Mass transfer through the liquid phase can be described by the film theory model (Porter, 1972); for binary mixtures, the mole fractions in the liquid bulk $x_{i,b}$ and at the interface $x_{i,I}$ are related to the molar fluxes by the following relationship

$$\frac{J_t}{k_L c_L} = \ln\frac{x_{i,I} - J_i/J_t}{x_{i,b} - J_i/J_t} \tag{7}$$

in which k_L is the mass-transfer coefficient in the liquid phase (m·s^{-1}), c_L is the molar concentration in the liquid phase (mol·m^{-3}).

Equations 3 to 7, coupled with the relationships describing the vapor-liquid equilibrium conditions existing at the interface, embody the mathematical description of the process. Once the expressions for both heat- and mass-transfer coefficients within the liquid phase h and k_L are available, the model can be used in a completely predictive way.

In the cases under consideration, the VOC composition in the distillate is much larger than in the liquid feed, so that a concentration polarization within the liquid phase is obtained, as usual. The VOC mole fraction at the interface $x_{i,I}$ is smaller than the corresponding bulk value $x_{i,b}$, and, consequently, the mole fraction of water at the interface is larger than in the bulk. Thus water transport results from a convective contribution pointing from the bulk to the evaporation surface, and a diffusive contribution pointing in the opposite direction. As a consequence, in general terms convective transport within the liquid phase cannot be neglected.

Discussion

The validity of the model presented in the previous section can be proved in two different but equivalent ways. For given operative conditions, first, the model equations can be used to predict the process performance in terms of total flux and separation factor. Secondly, the model is tested by comparing the predicted values for those quantities with the experimental data.

On the other hand, the test can be performed by comparing the heat- and mass-transfer coefficients, calculated through the model equations for each set of experimental data, with the corresponding values obtained by independent

models describing the transport phenomena in similar geometric configurations.

In the present work, the latter method is used in this section to discuss the influence of transport phenomena on the process, whereas the comparison between theoretical and experimental results is presented in the next section.

The heat- and mass-transfer coefficients for the membrane apparatus under consideration are evaluated as follows. Each set of experimental data at different feed flow rates provides for the average values of the total flux J_t and of the distillate composition $Y_{i,2}$; based on that, the vapor pressure P_I (Pa) and the interfacial vapor composition $Y_{i,I}$ can be calculated from Eqs. 4 and 3, respectively. From the model describing the liquid-vapor equilibrium, the temperature T_I (K) and the interfacial liquid composition $x_{i,I}$ are obtained. Van Laar, Wilson, and NRTL equations were used and their respective parameters were taken from Gmehling (1981). The average values for the coefficients h ($W \cdot m^{-2} \cdot K^{-1}$) and k_L ($m \cdot s^{-1}$) are finally calculated through Eqs. 6 and 7.

For all the mixtures used and for all the operating conditions inspected, the values obtained from the experimental data at various feed flow rates have been reported in the same figure (Figure 9), in terms of the relevant dimensionless groups. In particular in Figure 9a the Sherwood number is plotted vs. the Reynolds number, whereas in Figure 9b the Nusselt number is considered. The average numbers are defined as follows

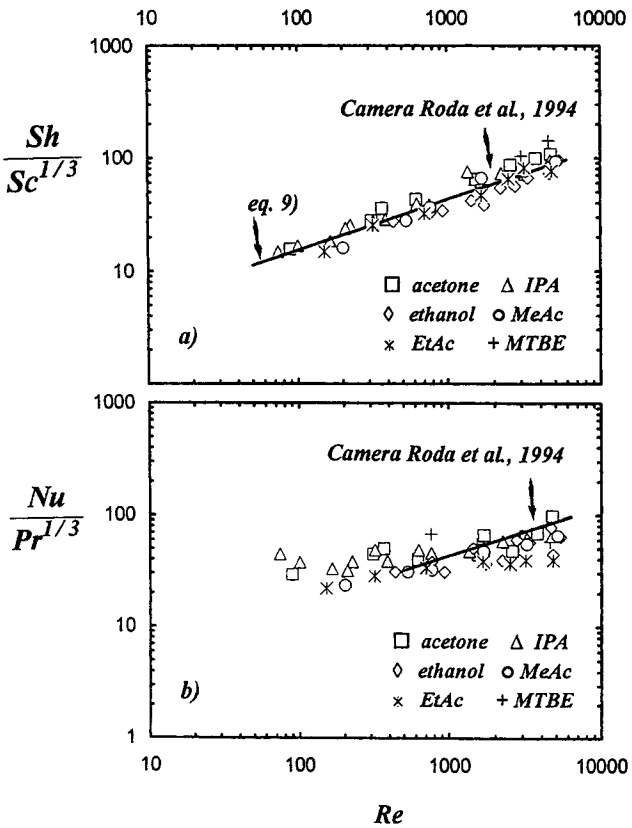

Figure 9. Sherwood and Nusselt numbers vs. Reynolds number: values obtained from VMD experiments at different feed flow rates.

$$Sh = \frac{k_L R_c}{\mathfrak{D}}, \quad Nu = \frac{hR_c}{k}, \quad Re = \frac{m_F}{2\pi b \mu} \tag{8}$$

where R_c (m) is the cell radius, b (m) the semicell thickness, and m_F ($kg \cdot s^{-1}$) the feed mass flow rate. The thermodynamic properties of the compounds are evaluated at the conditions existing in the bulk. Nu is the Nusselt number, $\mathfrak{D}$ is the diffusivity ($m^2\ s^{-1}$), k is the thermal conductivity ($W \cdot m^{-1} \cdot K$), and μ is the dynamic viscosity (Pa·s).

The mass-transfer data are well-fitted by the power law relationship

$$Sh = 1.80\ Re^{0.47} Sc^{1/3} \tag{9}$$

with a correlation coefficient of 91% and (Re is the Reynolds number). Sc is the Schmidt number. The maximum discrepancy between the experimental data and the fitting values is below 25%.

As it appears from the Reynolds dependence of the Sherwood number (Sh), nearly proportional to $Re^{0.5}$, the relationship for mass-transfer results is very similar to the one holding true for boundary layer over a flat surface. In any case the observed behavior clearly indicates that there is an appreciable concentration polarization confined in a thin layer close to the membrane.

The correlation represented by Eq. 9 is also in very good numerical agreement with the values obtained by an independent numerical model recently presented by Camera Roda et al. (1994) for circular cells with radial flow reported in Table 3. For the Re numbers in the range from 500 to 5,000, the numerical model gives practically the same results of the fitting relationships. In Table 3, v is the tube side velocity ($m \cdot s^{-1}$), GZ_m is the mass Graetz number, GZ_T is the thermal Graetz number, L is the fiber length (m), Pr is the Prandtl number, and α is the thermal diffusivity ($m^2 \cdot s^{-1}$).

With regard to the average Nusselt number, the data reported in Figure 9b do not present the same trend observed for the average Sherwood number. The wider dispersion observed is caused by the larger errors in the calculation of the heat-transfer coefficient through Eq. 6; indeed for the cases investigated, the interfacial temperature T_I is generally not very different from the bulk value T_b, so that significant errors are associated to the driving force $T_b - T_I$ and thus to the calculated heat-transfer coefficient. However, some considerations can be made on the basis both of the qualitative behavior observed and of the model reported as a comparison (Camera Roda et al., 1994) (Table 3). The Nusselt number seems to be rather constant in the lower Reynolds number region, thus indicating that the temperature profile is developed within the entire liquid phase and the temperature gradient is not simply confined in a thin layer adjacent to the membrane; at higher Reynolds values, on the contrary, there is a more significant thermal boundary layer effect.

We thus conclude that changes in the feed flow rate affect the process rate and separation, mostly through the changes induced in the concentration polarization and to a smaller extent through the changes induced in the temperature profiles.

Comparisons with data

The model reported in the previous section and represented by Eqs. 3 to 7 is used here first for a comparison with

Table 3. Transport Correlations for Flat and Hollow Fibers Geometries

Correlation	Flow	References
$Sh = 1.80 Re^{0.47} Sc^{1/3}$	$70 < Re < 5{,}000$	Cell with radial flow *Re*, *Sh* defined in Eq. 8 This work, Eq. 9
$j = 1.61 Re^{0.35}$ $j = \frac{Nu}{\left(\frac{R_c}{b}\right)^{1/3} Pr^{1/3}} = \frac{Sh}{\left(\frac{R_c}{b}\right)^{1/3} Sc^{1/3}}$	$500 < Re < 5{,}000$	Cell with radial flow *Re*, *Nu*, *Sh* defined in Eq. 8 (Camera Roda et al., 1994)
$Sh = \frac{k_L D}{\mathfrak{D}} = 1.62\, Gz_m^{1/3}$	$Gz_m > 20$	Hollow fibers; tube side; laminar flow $Gz_m = \frac{D^2 v}{\mathfrak{D} L}$ (Yang and Cussler, 1986)
$Nu = \frac{hD}{k} = 3.656$	$Gz_T > 20$	Hollow fibers; tube side; laminar flow; constant wall temperature $Gz_T = \frac{D^2 v}{\alpha L}$ (Knudsen and Katz, 1958)

experimental data and secondly for predictions of the membrane area required for a given separation.

Heat- and mass-transfer coefficients h and k_L are calculated according to the relationships from Camera Roda et al. (1994) reported in Table 3.

In Figures 6 and 7 the calculated fluxes of each component as well as the total flux are compared with the experimental data. Apparently, the model predictions are in good agreement with the experimental data. The model reproduces well the behavior of the total flux as well as the behavior of the flux of either permeating species vs. the downstream pressure, both in the low- and in the high-pressure range. In particular, the model correctly reproduces a significant feature observed, associated with the fact that at low-pressure values the water flux is dominant with respect to the solute flux, whereas at the higher pressures the total flux is practically given by the solute flux alone. Based on that, it seems convenient to work at relatively high pressures in the vacuum side, in order to obtain high solute concentration values in the distillate.

As an approximate indication obtained from Figures 6 and 7, the downstream pressure range at which the distillate shifts from water rich to solute rich is close to the vapor pressure P_w^* of pure water at the liquid bulk temperature; the same indication is also obtained from the data for acetone, IPA, and MTBE aqueous mixtures, although the corresponding figures are not explicitly reported here for the sake of simplicity. As a consequence, in that range distillate compositions are nearly 50 wt. % in correspondence with still relatively high solute flux values. The flux of the organic species remains practically constant for downstream pressures ranging from very low values up to values somewhat larger than P_w^*; the behavior observed suggests that the membrane area needed for a given organic removal should be nearly constant, working in a pressure range from zero up to values close to the water vapor pressure P_w^*.

Membrane area

The computation of the membrane area is performed for a VMD system in which the membrane apparatus consists of stages which can operate at different pressure values in the vacuum side; each stage is designed according to the scheme reported in Figure 10. Hollow fibers modules in a shell-and-tube configuration are connected in series, the liquid and vapor streams flow cocurrently, and the vapor permeate is collected at the pressure P_2 prevailing in the stage. (Subscript 2 is the vacuum side.)

Each module is designed by considering that in both phases temperature and composition change along the apparatus as in a plug flow; use of Eqs. 3 to 7 gives the following balance equations for the liquid stream

$$\frac{dn}{dA} = -J_t \tag{10}$$

$$\frac{d(nx_{i,b})}{dA} = -J_i \tag{11}$$

$$nc_p \frac{dT_b}{dA} = -\sum_i J_i \lambda_i \tag{12}$$

with the boundary conditions

$$n(0) = n_F, \quad x_{i,b}(0) = x_{i,F}, \quad T_b(0) = T_F \tag{13}$$

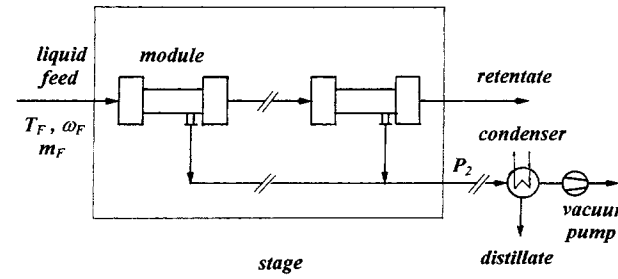

Figure 10. VMD pressure stage.

In Eqs. 10–13 c_p is the specific heat of the liquid phase ($J \cdot mol^{-1} \cdot K^{-1}$), and n is the molar flow rate ($mol \cdot s^{-1}$), while A represents the total interfacial area (m^2) of all the N_F capillaries contained in the module and is related to the axial coordinate z(m), so that

$$dA = \pi D_F N_F dz \tag{14}$$

N_F is the fibers number, and D_F is the fiber diameter (m). Analogous mass balance equations are considered for the vapor stream.

Explicit calculations of the membrane area needed for a desired separation have been performed for the reference case of benzene removal from water, a case of practical relevant interest. The apparatus considered uses Accurel Q3/2 PP hollow fibers (Table 1) arranged in modules 1 m long and presenting 50% packing density. These dimensions are constrained by the requirement of reducing the tube-and-shell side pressure drops.

Moreover, for a wide range of tube side velocities a laminar flow occurs so that the heat- and mass-transfer coefficients in the liquid phase greatly decrease along the module, according to the well-known Graetz model (Knudsen and Katz, 1958); for 0.5 m/s tube side velocity, modules 1 m long still give acceptable transmembrane fluxes in the outlet section.

Standard relationships are used to calculate the transport coefficients in the liquid phase (Table 3), by assuming, as usual, that velocity profiles inside the fibers are not significantly altered by convective mass transfer. In view of the very short entry length for heat transfer, the heat-transfer coefficient is calculated with reference to a completely developed temperature profile, whereas the local mass-transfer coefficient is obtained in accordance with the fact that the entry region for mass transfer is longer than the whole module length.

Figure 11 shows the membrane area required for various benzene removals in a single pressure stage through VMD of aqueous mixtures containing 1,000 ppm benzene. The data are reported vs. the VMD pressure degree of the stage, φ, defined as the ratio between the stage pressure P_2 and the water vapor pressure at the feed conditions T_F

$$\varphi = P_2 / P_w^*(T_F) \tag{15}$$

Apparently, at P_2 values lower than the water vapor pressure the membrane area is independent of the downstream pressure; at higher values, on the contrary, the membrane area needed for a given removal progressively increases, as the driving force decreases.

Since it is generally highly desirable to work at P_2 values as high as possible, in order to reduce operating costs based on the results shown in Figure 11 attractive working pressures are thus apparent, ranging roughly from $\varphi = 0.9$ to $\varphi = 1.2$; the upper limit 1.2 is qualitatively identified by the pressure value above which a sharp decrease of the driving force takes place; the lower limit 0.9 is qualitatively indicated based on the values below which too high water fluxes are obtained, thus demanding high energy consumption for the evaporation of water and producing very high shell side pressure drops.

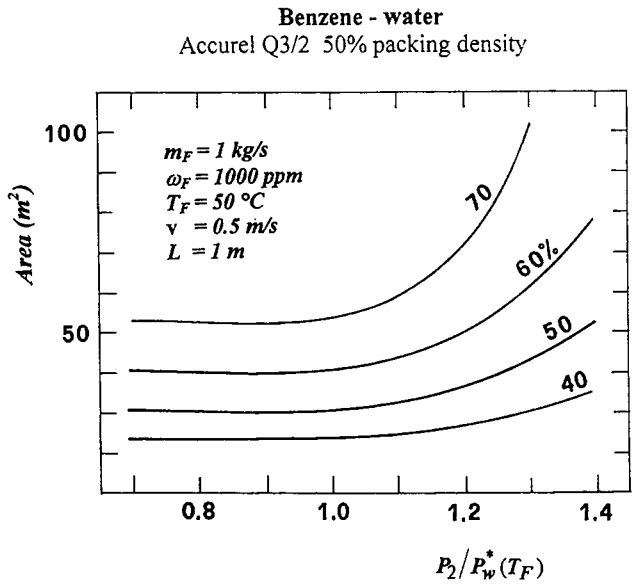

Figure 11. VMD of benzene-water mixtures: membrane area vs. pressure degree with benzene removal as a parameter.

In that working range an optimal pressure value can be obviously identified on the basis of economic considerations. Indeed, at the lower-pressure values higher water fluxes and lower concentrations in the distillate are obtained with respect to the values achievable at the higher pressures; as a consequence, the plant investment and operating costs, associated to the sections downstream the membrane apparatus, may give very different contributions to the overall separation cost at the different values of the downstream pressure P_2.

Conclusions

The VMD process was experimentally studied as a separation technique to extract VOCs from aqueous streams. Flat membrane apparatuses were used with radial flow in both feed and permeate sides. Several organic components have been considered both with complete and partial miscibility in water. The effect of the downstream pressure on the process performance has been examined in some detail, as well as the influence of changes in the feed flow rate at different temperatures and at different VOC feed concentrations.

The typical operation conditions for VMD consist in permeate pressure values always smaller than the saturation pressure in order to prevent condensation; reducing the permeate pressure results in all cases in an increase in the overall permeate flux, however, there is correspondingly a remarkable decrease in the separation factor of the process. Conversely by increasing the downstream pressure, very interesting rises in the VOC concentration in the permeate stream were obtained up to values exceeding 70 wt. % for feed concentration around 2 wt. %.

As a general indication, we can say that for downstream pressures above the vapor pressure of water, the permeate flux becomes richer and richer in the VOC while increasing the pressure up to values slightly larger than the vapor pressure of pure water, thus leading to rather high vaporization

factors. In most of the cases inspected, the remarkable increase in the permeate VOC concentration was paralleled by only minor decreases in the VOC permeation flux. Of course, the pressure range in which the downstream pressure may be varied is broadened by increasing the operating temperature.

As typically observed in all other membrane distillation processes, fluxes increase almost exponentially with increasing temperature.

As a general trend, an appreciable permeation rate increase is observed in all cases with increasing the feed flow rate; that is a clear indication of the relevance of the resistances offered to the transport phenomena by the liquid feed. In particular, it was pointed out that the flux of water is much less sensitive to changes in the feed flow rate than the flux of the organic component; in the latter case, both heat- and mass-transfer resistances affect the evaporation rate, due to concentration and temperature polarization effects. For the water flux, vice versa, only temperature polarization plays an appreciable role in view of the concentration range considered.

For the process, a mathematical model description has been also considered, which accounts for the relevant transport resistances contributing to the separation rate and efficiency, namely, heat- and mass-transfer resistances within the liquid feed and mass-transfer resistance through the membrane. The latter is rather simply associated to the permeability of the microporous membrane K_m in the prevailing Knudsen regime; K_m was measured directly through independent tests.

The liquid-phase resistances are associated to the transport of the organic species from the liquid bulk to the evaporation interface located at the membrane surface, as well as to the heat transfer toward the membrane/liquid interface, which provides for the energy supply demanded by the evaporation process.

For the radial flow prevailing in the feed side of the apparatus, the heat- and mass-transfer coefficients were calculated from the experimental data and proved to be satisfactorily consistent with the values obtained by independent model descriptions.

The model developed correctly describes all the features of the process. In particular, it reproduces well the relevant behavior observed for both water and organic fluxes vs. the vacuum side pressure.

The computation of the membrane area needed in a VMD system, designed with reference to hollow fibers, puts in evidence the crucial role of the pressure in the process performance.

The working pressure values suitable for a more convenient process conduction range approximately from 0.9 to 1.2 times the water vapor pressure at the feed conditions. In that range, the process is characterized by a rather small driving force for water evaporation, simultaneously preserving a still high value for the organic compound.

Acknowledgments

This work was partially supported by CNR grant 91.01756H3 and by the Italian Ministry of University and Scientific Research (MURST 60%).

Literature Cited

Andersson, S. I., N. Kjellander, and B. Rodesjo, "Design and Field Tests of a New Membrane Distillation Desalination Process," *Desalination*, **56**, 345 (1985).

Aptel, Ph., E. Julien, N. Ganne, R. Psaume, Y. Aurelle, and M. Roustan, "Pervaporation Situation Among Other Competitive Techniques in Halogenated Solvents Removal From Drinking Water," *Proc. 3rd Int. Conf. on Pervaporation in Chem. Ind.*, Nancy, France, R. Bakish, ed., pp. 463–475 (Sept. 19–22, 1988).

Bandini, S., C. Gostoli, and G. C. Sarti, "Separation Efficiency in Vacuum Membrane Distillation," *J. Memb. Sci.*, **73**, 217 (1992).

Bandini, S., G. C. Sarti, and C. Gostoli, "Vacuum Membrane Distillation: Pervaporation Through Porous Hydrophobic Membranes," *Proc. 3rd Int. Conf. on Pervaporation in the Chem. Ind.*, Nancy, France, R. Bakish, ed., p. 117 (Sept. 19–22, 1988).

Camera, Roda G., C. Boi, and G. C. Sarti, "Heat and Mass Transfer Boundary Layers in Radial Creeping Flow," *Int. J. Heat and Mass Transf.*, **37**, 2145 (1994).

Dullien, F. A. L., *Porous Media-Fluid Transport and Pore Structure*, Academic Press, London (1979).

Gmehling, J., Chemistry Data Series, Dechema, Frankfurt (1981).

Gostoli, C., G. C. Sarti, and S. Matulli, "Low Temperature Distillation through Hydrophobic Membranes," *Sep. Sci. and Technol.*, **22**, 855 (1987).

Hofman, E., D. M. Pfenning, E. Philippsen, P. Schwahn, M. Sieber, R. Wehn, and D. Woermann, "Evaporation of Alcohol/Water Mixtures Through Hydrophobic Porous Membranes," *J. Memb. Sci.*, **34**, 199 (1987).

Jonsson, A. S., R. Wimmerstedt, and A. C. Harrysson, "Membrane Distillation—A Theoretical Study of Evaporation Through Microporous Membranes," *Desalination*, **56**, 237 (1985).

Knudsen, J. G., and D. L. Katz, *Fluid Dynamics and Heat Transfer*, Chem. Eng. Ser., McGraw-Hill, New York (1958).

Lipski, C., and P. Cotè, "The Use of Pervaporation for the Removal of Organic Contaminants from Water," *Environ. Prog.*, **9**, 254 (1990).

Porter, M. C., "Concentration Polarization with Membrane Ultrafiltration," *I&EC Product Res. and Dev.*, **11**, 234 (1972).

Sarti, G. C., and C. Gostoli, "Separation of Liquid Mixtures by Membrane Distillation," *J. Memb. Sci.*, **41**, 211 (1989).

Sarti, G. C., C. Gostoli, and S. Bandini, "Extraction of Organic Components from Aqueous Streams by Vacuum Membrane Distillation," *J. Mem. Sci.*, **80**, 21 (1993).

Sarti, G. C., C. Gostoli, and S. Matulli, "Low Energy Cost Desalination Processes Using Hydrophobic Membranes," *Desalination*, **56**, 277 (1985).

Schofield, R. W., A. G. Fane, and C. J. D. Fell, "Heat and Mass Transfer in Membrane Distillation," *J. Memb. Sci.*, **33**, 299 (1987).

Wijmans, J. G., J. Kaschemekat, J. E. Davidson, and R. W. Baker, "Treatment of Organic-Contaminated Wastewater Streams by Pervaporation," *Environ. Prog.*, **9**, 262 (1990).

Yang, M., and E. L. Cussler, "Designing Hollow-Fiber Contactors," *AIChE J.*, **32**, 1910 (1986).

Manuscript received Dec. 20, 1994, and revision received July 26, 1996.